Unraveling Dipolar Regime and Kerker Conditions in Mid-index Mesoscale Dielectric Materials

Brighton Coe[1,†], Jorge Olmos-Trigo[2,†,‡], Dylan Qualls[1], Minani Alexis[1], Michal Szczerba[1], Diego R. Abujetas[3], Mahua Biswas[1], and Uttam Manna[1,]*

[1]Department of Physics, Illinois State University, Normal, Illinois 61709, United States
[2]Donostia International Physics Center (DIPC), Donostia-San Sebastián, 20018, Spain
[3]Physics Department, Fribourg University, Chemin de Musée 3, Fribourg 1700, Switzerland

Keywords: nanophotonics, mesoscale interactions, mid-index materials, optical anapole, zero backscattering, optical spectroscopy

Nanophotonic phenomena, such as zero optical back scattering, nonradiating anapole states, *etc.* are related to the excitation of single dipolar modes – hence so far, they have only been observed within a few relatively high-index dielectric materials (refractive index, $n > 3.5$) in the nanoscale regime at the optical frequencies. Here, we unravel dipolar regime, demonstrate close-to-zero backscattering, and excite optical anapoles in mid-index dielectric spheres (titanium di-oxide, TiO_2; $n \sim 2.6$) at the mesoscale regime (particle diameter, $d \sim$ incident wavelength, λ) under illumination with tightly focused Gaussian beams (TFGBs). We observe successive minima associated with dipolar excitation satisfying the first Kerker condition in the scattering spectra of single TiO_2 spheres with diameters in the micrometer range. Moreover, at specific wavelengths, the electric and magnetic dipolar scattering amplitudes of the dielectric microspheres simultaneously go close-to-zero leading to the excitation of hybrid optical anapoles with the total scattering intensity ~ 5 times weaker for TFGB illumination with numerical aperture, NA ~ 0.95 vs. 0.1. Our result pushes the boundary of observation of nanophotonic phenomena to new regime with regards to type and size of the materials.

† Both these authors contributed equally to this work.
‡ Email: jolmostrigo@gmail.com
* Email: umanna@ilstu.edu

1. Introduction

The field of nanooptics/nanophotonics[1] is usually associated with plasmonic structures made of noble metals (such as Gold, Silver, *etc*.) that are well known to enhance electromagnetic fields at the nanoscale. Recently, high refractive-index dielectric nanostructures have generated a lot of interest as alternative building blocks of all-dielectric metamaterials and optical devices because of their reduced dissipative losses and large resonant enhancement of both the electric and magnetic near-fields[2-4]. Because of their low losses and strong electromagnetic response, the resonant excitation of dielectric nanostructures offers a unique playground to demonstrate new nanophotonic effects. These include, but are not limited to nonradiating anapole states[5,6], zero optical backscattering leading to optimum forward scattering[7,8], magnetic hotspot enhanced Purcell effect[9,10], surface enhanced Raman scattering[11], and nanoantenna[12,13].

However, most of these novel nanophotonic effects observed in high refractive-index lossless dielectric materials are related to the excitation of single dipolar modes – hence so far, they have only been observed in the nanoscale regime at the optical frequencies. In contrast, in the mesoscale regime (where the particle diameter, d is approximately equal to the wavelength of the incident light, λ), these effects are inaccessible due to the contributions from higher order multipolar modes under plane wave (PW) illumination. Recently, there is a growing interest in the study of optical phenomena at mesoscale regime with low refractive index ($1< n <2$) structures, termed as Mesotronics[14]. In these low-index wavelength-scaled dielectric particles, the electromagnetic fields are enhanced by the interference effects between the different field components generated in or/and near the particle[14]. Even though, the localized field is limited to the particle size of the order of $d > \lambda$, a number of interesting phenomena and applications have been observed in these low-index dielectric particles. For example, strong molecule-cavity coupling[15], optical singularities that form two extreme hotspots near the particle poles[16], higher order Fano resonances that provide giant magnetic field leading to super-oscillation effects[17,18], the whispering gallery mode effect overcoming the diffraction limit leading to super-resolution imaging[19], structured fields in the form of photonic hook and loops allowing new class of 'on-chip' optical traps for anisotropic nanoobjects[20], *etc*. indicate promising new directions of research enabled by low-index mesoscale dielectric particles.

Recently, it was theoretically predicted[21,22], one can unravel dipolar regimes in a homogenous lossless dielectric sphere with a wide range of size parameter and several refractive indices (*n)* under illumination with a pure dipolar field (PDF). More specifically, it was shown that the sectoral and propagating illumination of PDF with well-defined handedness or helicity ($\sigma = \pm 1$) excites only electric and magnetic dipolar modes for several refractive indices with a wide range of size parameters beyond the limit of small particles, *i.e*., $x\ (= 2\pi(r/\lambda))$-size parameter > 2, where r is the radius of the particle [21,22].

Moreover, the calculation of asymmetry parameter (g-parameter), defined as the ratio of the cosine-weighted scattering cross section over the total scattering cross section, in the dipolar regime shows that

successive first Kerker conditions[23] exist for several refractive indices at the mesoscale regime.[21,22] Furthermore, it was also shown that emergence of pure electric or magnetic scattering regimes can give rise to zero total scattering efficiency, which are associated with excitation of nonradiating optical anapoles for several refractive indices at the mesoscale regime.[21] Note that the first Kerker condition leads to perfect zero backscattering, regardless of the size of the sphere, when the condition $\varepsilon = \mu$ is satisfied, where ε is the relative permittivity, and μ is the permeability.[7,8,23] Control over directionality of scattered radiation is an important step towards design of nano and mesoscopic photonic devices, where maximum transmission of light into the receiver is desired in order to store as much radiation energy as possible[24].

On the other hand, nonradiating anapoles are special configurations of charge-current distributions that do not radiate in the far-field[25,26]. Historically, nonradiating sources have attracted a lot of attention in the field of quantum mechanics in the context of radiationless motion[27], extended electron models[28], as well as providing possible scenarios for observing a dynamic Aharonov-Bohm effect[29]. Recently, there is a growing interest in nonradiating sources in nanophotonics and quantum optics because of their ability to highly confine electromagnetic fields in subwavelength structures[5,6,30-33]. Note that the anapoles are not inherent states of a resonant structure but a dynamic excitation, which depends strongly on external parameters such as the excitation geometry or properties of the incident beam[5,32-34]. It has been predicted that efficient excitation of the nonradiating anapole states can give rise to enhanced nonlinear effects[35-37], nanolasers[38], ideal magnetic scattering [39], broadband absorption[40], sensing[41], metamaterials and metasurfaces[42], and extremely high Q-factors ($\sim 10^6$)[43-46].

In general, all-dielectric materials (ADMs) are classified into three types based on different optical resonant modes changing with refractive index; namely high-index, mid-index and low-index materials.[47] The high-index ADMs are classified with refractive index greater than 3.5, the mid-index ADMs are classified with refractive index between 2 to 3.5, and low-index ADMs are classified with refractive index smaller than 2.[47] Nevertheless, excitation of electric and magnetic dipolar modes and their associated novel nanophotonic effects, such as optical anapoles, zero backscattering, *etc*. are currently restricted to a few relatively high refractive-index materials ($n > 3.5$) at the nanoscale regime – typically within silicon, germanium, and gallium arsenide nanoparticles. Here, we experimentally unravel dipolar regime, demonstrate close-to-zero backscattering, and excite non-radiating anapole states in mid-index titanium di-oxide (TiO_2, $n \sim 2.6$) dielectric spheres at the mesoscale regime under illumination with tightly focused Gaussian beams (TFGBs) for the first time. We observe successive minima in the scattering spectra of single TiO_2 microspheres with diameter, $d \sim 0.78$ μm, and 0.88 μm with the scattering intensity almost reaching zero. The calculation results show that these scattering minima are associated with dipolar electric and magnetic modes satisfying the first Kerker condition. Moreover, at specific wavelengths, for example $\lambda \sim 590$ nm for $d \sim 0.78$ μm, and $\lambda \sim 665$ nm for $d \sim 0.88$ μm, the electric and magnetic scattering amplitudes

simultaneously go to zero leading to the excitation of hybrid optical anapoles with the total scattering intensity ~ 5 times weaker for TFGB illumination (numerical aperture, NA ~ 0.95) compared to the intensity for lower NA (NA ~ 0.1) illumination with beam characteristics similar to plane waves.

2. Results and Discussion

2.1 Theoretical Considerations

The selective excitation of electric and magnetic dipolar modes under PDF illumination can be explicitly derived from the multipole expansion of the circularly polarized PW,[21,48]

$$\frac{\boldsymbol{E}_{\sigma}^{(PW)}}{E_0} = \frac{\hat{\boldsymbol{x}}+i\sigma\hat{\boldsymbol{y}}}{\sqrt{2}} e^{ikz} = \sum_{l=0}^{\infty}\sum_{m_z=-l}^{+l} C_{lm_z}^{\sigma}\boldsymbol{\Psi}_{lm_z} \quad (1)$$

Here, $C_{lm_z}^{\sigma} = \sigma i^l\sqrt{4\pi(2l+1)}\delta_{m_z\sigma}$ are the PW coefficients and $\boldsymbol{\Psi}_{lm_z}$ denotes the vector spherical wavefunctions (VSWFs).[49] These VSWFs are simultaneous eigenvectors of the square of the total angular momentum, J^2, the z components of the total angular momentum, J_z and the helicity operator for the monochromatic waves, Λ, with eigenvalues $l(l+1), m_z$ and σ, respectively[50]. The sectoral and propagating illumination of spheres with PDF with well-defined J^2, J_z, and Λ with eigenvalues $l = 1, m_z = \sigma = \pm 1$, only excites electric and magnetic dipoles, respectively. Note that this phenomenon stems from the fact that, for particles placed at the focus, the only multipoles that are present in the incident beam can be excited within the particle, as has been previously demonstrated by tailoring multipolar Mie scattering using Cylindrical Vector Beams[51,52] and changing the helicity and angular momentum of the incident beam[53].

The *g*-parameter of a lossless dielectric sphere under PDF illumination can be written as [21],

$$g = \frac{Re[a_1 b_1^*]}{|a_1|^2+|b_1|^2} = \frac{\sin\alpha_1 \sin\beta_1 \cos(\alpha_1-\beta_1)}{sin^2\alpha_1 + sin^2\beta_1} \quad (2)$$

where $a_1 = i\sin\alpha_1 e^{-i\alpha_1}$ and $b_1 = i\sin\beta_1 e^{-i\beta_1}$ denote the electric and magnetic Mie coefficients, respectively[54]. Moreover, the expected value of the helicity, $\langle\Lambda\rangle$, and the ratio between the backward and forward scattering cross sections, Q_b/Q_f are determined by the *g*-parameter under a PDF illumination with well-defined helicity ($\sigma = \pm 1$, the left polarized light is $\sigma = +1$, positive helicity), as [21,55]

$$\frac{Q_b}{Q_f} = \frac{1-\langle\Lambda\rangle}{1+\langle\Lambda\rangle}, \text{ with } \langle\Lambda\rangle = 2g \quad (3)$$

To get a deeper understanding of the scattering properties of the dielectric spheres under PDF illumination, the *g*-parameter (Eq. 2 above) was calculated as a function of the dipolar electric and magnetic scattering phase-shifts.[21] The results showed that the first Kerker condition ($g = 0.5;\ \langle\Lambda\rangle = +1$) is satisfied for several $y = (nx)$ - parameters with $y > 4.5$ for PDF illumination. More specifically, it was shown that one can practically obtain zero backscattering at any frequency in the optical regime, for $y \approx 4.6,$ $7.3\ \ 9.2, 12.1, 13.9$ for a lossless sphere under TFGB illumination. For example, for TiO_2 sphere, for $y =$

9.2, one should be able to obtain zero back scattering at any frequency in the optical regime by varying the diameter from 0.48 to 0.98 μm. Furthermore, excitation of lossless dielectric spheres under PDF illumination revealed another interesting phenomenon – the emergence of pure electric (or magnetic) scattering regimes for $\sin\beta_1 = 0$ (or $\sin\alpha_1 = 0$), which give rise to $g = 0$, according to Eq. (2) [21]. More specifically, it was shown that the scattering efficiency vanishes when the electric and magnetic scattering amplitude simultaneously go to zero, for several $n = 1.72,\ 2.43,\ 3.13,\ 3.83$, and for a wide range of $y\ (= nx)$-size parameter ($6 < y < 14.5$) under PDF illumination[21]. These singularities in the g-parameter are non-radiating states referred to as hybrid or Kerker anapoles that appear as analytical solutions of the first Kerker condition with zero scattering yet enhanced internal energy.

Here, the calculations were performed using the widely used generalized Lorentz-Mie theory (GLMT). Explicit analytical formulas have been extracted directly from Ref [[56]]. The electric and magnetic Mie coefficients were taken from Bohren and Huffmann[57] to solve the exact problem of a Gaussian beam incident on a homogeneous dielectric sphere.

2.2 Experimental Considerations

Even though sectoral and propagating dipolar beams fulfill Maxwell's equations[48], it has not been experimentally implemented yet[58-60]. Alternatively, it was shown that the TFGBs [56,61-63] can mimic the scattering properties under PDF illumination [21]. This is based on the engineering of the multipolar content of the incident beam with beam coefficients $C_{lm_z}^{\sigma}$. In this approach, TFGB can be used to select a few relevant Mie coefficients, and control the relative weight of the different multipolar modes (given by a_l and b_l) with the use of the multipolar content of the incident field [56]. The independent control of both angular momentum and polarization allows for the generation of a Gaussian Beam with $m_z = \sigma = 1$. In this case, the relative weight of each multipolar order with respect to the dipolar order can be highly minimized when the beam is tightly focused at the center of the object. The relative weights of each C_{l11} multipolar order for NA = 0.95 and 0.1 with respect to the dipolar contribution are shown in Fig. 1a. The scattering efficiency of a sphere illuminated by a TFGB with well-defined helicity can be written as [21,56]

$$Q_{sca}^{GB} = \sum_{l=1}^{\infty} \frac{(2l+1)}{x^2} |C_{l11}|^2 (\sin^2\alpha_l + \sin^2\beta_l)\,. \qquad (4)$$

The value of the beam shape function, C_{l11} heavily decreases as the multipolar order l is increased. In fact, for NA = 0.95, the relative weight of the dipolar content of the incident beam is ~ 80%, and the quadrupolar contribution and higher multipolar orders represent ~ 20% of the content of the incident beam as shown in Fig.1a. Therefore, the TFGBs are dominantly dipolar in nature.

To unravel dipolar regimes, demonstrate zero backscattering, and excite hybrid optical anapoles in mid-index dielectric microspheres, we have developed a TFGB spectroscopy set-up as shown in Fig.1b. In this

set-up, the output of a white light continuum is coupled to an inverted optical microscope equipped with a high NA objective lens. For creating a tightly focused beam at the sample plane, we used a 40×, NA = 0.95 objective (Olympus, UPLXAPO). Moreover, for control experiments, the diameter of the beam was changed by inserting two Irises in the beam path as to measure the scattering spectra for low NA illumination. The back-scattered spectra (angular range determined by the NA of the microscope objective) are acquired by an EM-CCD (Andor Newton) connected to an imaging spectrometer (Shamrock 303i) coupled to the side port of the microscope. Note that the supercontinuum laser exhibits different laser spot sizes as a function of wavelength. We have taken into account while calculating the beam shape coefficients as described elsewhere.[64] Within our measurement window (500 – 780 nm), the variation of the spot size as a function of wavelength was found to be negligible. Commercially available[65] TiO_2 microspheres synthesized using isopropyl titanate hydrolysis method with precisely controlled uniform particle size and narrow size distribution with diameter, $d = 0.5 - 1.0\ \mu m$ was used for our experiments. The Scanning Electron Microscope (SEM) image and x-ray diffraction spectrum of the TiO_2 microspheres are shown in Fig. S1 in the Supplementary Information (SI). The XRD results reveal that the TiO_2 microspheres are anatase crystals in nature, which is known to have a refractive index $n \approx 2.6$ [66].

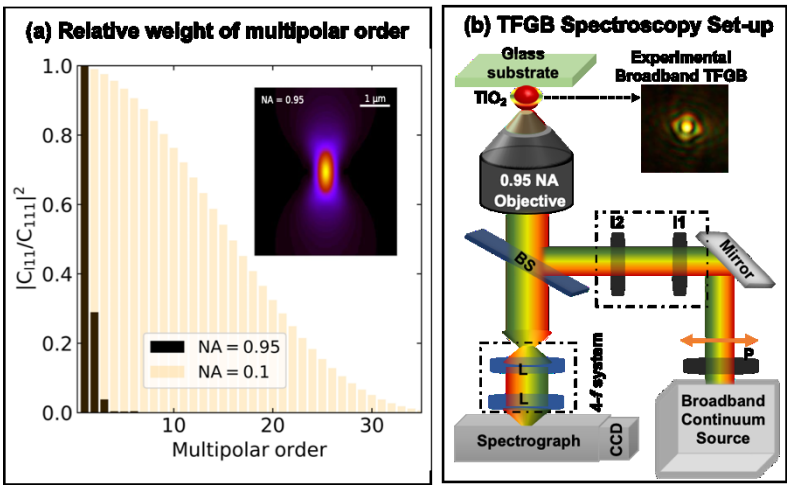

Figure 1: (a) Relative weight of the multipolar order for NA = 0.95, and 0.1 with respect to the dipolar contributions. The inset shows an image of propagating TFGB in the vertical direction with NA = 0.95. (b) Schematics of the TFGB spectroscopy set-up. BS → Beam Splitter; L→ Lens; I→ Iris; P→ Polarizer. The inset shows an image of the experimentally generated broadband TFGB propagating out of the page with NA ~ 0.95.

2.3 Excitation of Dipolar Regime and Close-to-Zero Backward Scattering

Colloidally synthesized micro/nanospheres suffer from inhomogeneities in nanoparticle size and shape, which cause variations in the spectral responses. As a result, the interpretation of the scattering spectra at

the single particle level requires a correlated SEM and optical microscopy approach [52,67,68]. In this approach, diluted solution of the microspheres is drop-casted on a patterned glass substrate, and optical spectra are measured at the single nanostructure level by correlating the optical and SEM images as shown in Fig. S2 in the SI. The insets of Figs. 2a and 2b show the SEM images of the exact same microspheres whose scattering spectra are shown in Figs. 2a and 2b, respectively. From the SEM images of Figs. 2a and 2b, the diameter of the single TiO_2 microspheres, d is found to be ~ 0.78 μm, and ~ 0.88 μm, respectively.

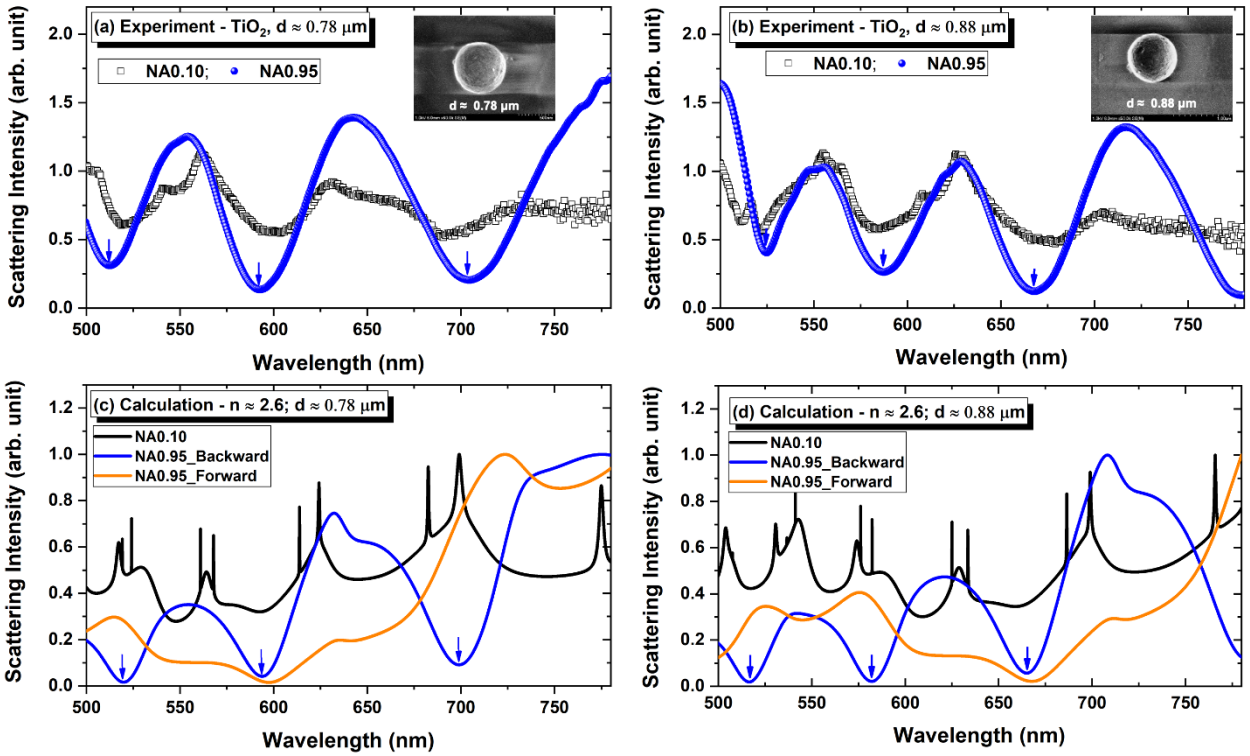

Figure 2: Experimentally measured (a, b) and calculated (c, d) scattering spectra of a single TiO_2 microsphere with d ~ 0.78 μm (a, c) and d ~ 0.88 μm (b, d) under TFGB illumination with NA = 0.95 and 0.10. The insets of (a) and (b) show the SEM image of the exact same single microspheres whose scattering spectra are shown in (a) and (b) respectively. For NA ~ 0.95, both experimental and calculated backward scattering spectra show several scattering minima, at λ ~ 515 nm, 590 nm, 700 nm for d ~ 0.78 μm (a, c); and at λ ~ 515 nm, 585 nm, 665 nm for d ~ 0.88 μm (b, d), which are associated with the first Kerker condition. The scattering minima at λ ~ 590 nm for d ~ 0.78 μm, and at λ ~ 665 nm for d ~ 0.88 μm are associated with excitation of hybrid optical anapoles.

Figs. 2a and 2b show the experimental scattering spectra of a single TiO_2 microspheres for d ~ 0.78 μm, and 0.88 μm, respectively, measured in the backward direction for a limited angular range determined by the NA of the objective lens under TFGB illumination with NA ~ 0.95 and 0.1. Figs. 2c and 2d show the calculated forward and backward scattering spectra of a single TiO_2 microsphere for d ~ 0.78 μm, and

0.88 μm, respectively under TFGB illumination with NA ~ 0.95 and 0.1. The experimental and calculated backward scattering spectra for NA = 0.95 show that several scattering minima, at λ ~ 515 nm, 590 nm, 700 nm for d ~ 0.78 μm (Figs. 2a and 2b); and at λ ~ 515 nm, 585 nm, 665 nm for d ~ 0.88 μm (Figs. 2c and 2d) appear within the measurement window (λ = 500 – 780 nm) as indicated by the blues arrows. This series of scattering minima in the experimental and calculated backscattered spectra are associated with the first Kerker condition when $\alpha_1 = \beta_1$ is satisfied, as it has been theoretically predicted in [21].

To get a deeper insight into these results, we have performed multipolar decomposition of the total scattering spectra of TiO_2 microspheres with d ~ 0.78 μm under TFGB illumination with NA ~ 0.1 and 0.95 as shown in Figs. 3a, and 3b, respectively. The results of the multipolar decomposition for TiO_2 microspheres with d ~ 0.88 μm are shown in Fig. S3 in the SI. The calculation results show that, for NA = 0.10, the contributions from the dipolar, quadrupolar and, octopolar electric and magnetic modes do not add up to the total scattering intensity. In fact, for NA = 0.10, the total scattering spectra are dominated by the multipolar orders $3 < l < 10$ in the optical regime. On the other hand, for NA = 0.95, the scattering spectra are dominated by the dipolar electric and magnetic modes with small contributions from the quadrupolar and octopolar modes. These results signify that one can indeed unravel dominant dipolar regime in a homogenous lossless dielectric sphere under TFGB illumination.

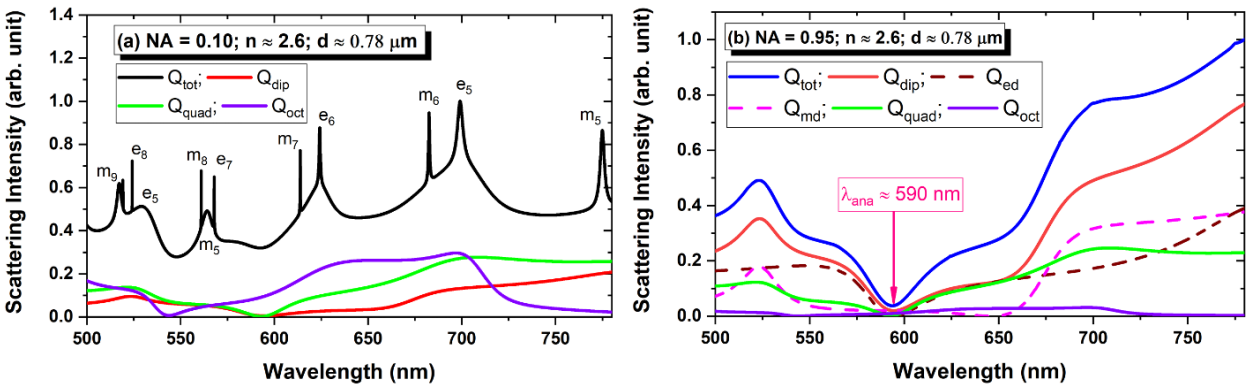

Figure 3: Multipolar decomposition of the total scattering spectra of TiO_2 microspheres with d ~ 0.78 μm under TFGB illumination with NA = 0.10 (a) and NA = 0.95 (b). For NA = 0.10 (a), the total scattering spectrum is dominated by the multipolar order 3 < l < 10. For NA = 0.95 (b), the total scattering spectrum is dominated by the contributions from dipolar electric and magnetic modes. Also, the scattering minima associated with the total, electric, and magnetic dipolar scattering coincide with each other, at λ_{ana} ~ 590 nm leading to the excitation of hybrid optical anapole in this regime.

Note that excitation of dipolar regime and the associated effects under TFGB illumination requires placing the single microspheres at the focal plane of the incident beam. Therefore, to ensure the presented scattering spectra are obtained by placing the single microspheres at the focal plane, the particle is raster scanned across the focal plane while recording the scattering spectra. A set of representative roaster scan

spectra of the TiO_2 microsphere with $d \sim 0.78$ μm is shown in Fig. S4 in the SI. Also, note that we could not experimentally measure scattering spectra in the forward direction as such measurement would require integration of an upright microscope on top of the existing inverted microscope (condenser cannot be used to create tightly focused incident beam), which is not readily available to us.

2.4 Excitation of Optical Anapoles

The scattering minima at $\lambda \sim 590$ nm for $d \sim 0.78$ μm (Figs. 2a, and 2c), and at $\lambda \sim 665$ nm for $d \sim 0.88$ μm (Figs. 2b, and 2d) in the backscattered spectra nearly coincide with the scattering minima of the forward scattering spectra under illumination with NA ~ 0.95 as shown in Figs 2c and 2d. The results of the multipolar decomposition show that the scattering minima associated with the total (Q_{tot}), and electric dipolar (Q_{ed}) and magnetic dipolar (Q_{md}) scattering coincide with each other, at $\lambda_{ana} \sim 590$ nm for $d \sim 0.78$ μm (Fig. 3b), and $\lambda_{ana} \sim 665$ nm for $d \sim 0.88$ μm (Fig. S3b). Since the total scattering efficiency almost vanishes due to simultaneous disappearance of the electric and magnetic scattering amplitudes at these wavelengths, we can conclude that these scattering minima are associated with excitation of hybrid optical anapoles ($\sin\beta_1 = \sin\alpha_1 = 0$) within homogenous lossless dielectric microspheres under TFGB illumination. Note that for NA = 0.1, in addition to the scattering minima, several scattering peaks also appear in the scattering spectra in the optical regime. However, the total scattering intensity associated with these minima is approximately ~ 5 times weaker for illumination with NA ~ 0.95 vs. 0.1 as deduced from the experimental spectra of Figs. 2(a) and 2(b).

We note that even though the total scattering intensity is dominated by dipolar scattering under TFGB illumination with NA = 0.95, there are contributions from the quadrupolar (Q_{quad}) and octopolar (Q_{oct}) scattering in the total scattering intensity. These can be attributed to the non-ideal dipolar excitation that occurs under TFGB illumination; for NA = 0.95, the relative weight of the dipolar content ~ 80% as discussed in Section 2.2. Moreover, for an ideal anapole excitation, one would expect the total scattering intensity to completely vanish ($Q_{scat} = 0$) at the anapole wavelength (λ_{ana}). Even though, Q_{scat} is very close to zero, it does not completely vanish in our case. In addition to the non-ideal dipolar character of the TFGB illumination, we attribute this to the different value of the refractive index of TiO_2 microspheres used in the experiment ($n \approx 2.6$) compared to the theoretically predicted value of the refractive index ($n \approx 2.43$) that is expected to give rise to ideal hybrid optical anapoles in this regime [21]. To verify this, we have calculated the forward and backward scattering intensity for a microsphere with $d = 0.78$ μm and $n = 2.43$ under PDF illumination as shown in Fig. S5 in the SI. The results show that excitation of a microsphere with $n = 2.43$ under PDF illumination indeed leads to excitation of ideal optical anapoles with the total scattering intensity reaching zero at the anapole wavelength, as predicted theoretically.

Another important aspect of optical anapoles is that, even though the scattering amplitude becomes zero, the energy density is non-zero, which means that the energy is concentrated inside the particle [5,6,32,33,52,69]. To verify this, we have also calculated the internal electromagnetic energy from the internal electric and magnetic fields, $\boldsymbol{E}^{int}$, and $\boldsymbol{H}^{int}$ using the internal Mie coefficients under TFGB illumination, given by [21],

$$\frac{W^{int}}{W^{i}} = \epsilon_r \frac{\int\left(|\boldsymbol{E}^{int}|^2 + Z^2|\boldsymbol{H}^{int}|^2\right)dV}{\int\left(|\boldsymbol{E}^{i}|^2 + Z_0^2|\boldsymbol{H}^{i}|^2\right)dV}, \tag{5}$$

where $\varepsilon_r = n^2$, $Z = \sqrt{\mu/\epsilon} = (1/n)\sqrt{\mu_0/\epsilon_0} = Z_0/n$. Here, $\frac{W^{int}}{W^{i}}$ is normalized to the focal energy when the sphere is absent. The $\frac{W^{int}}{W^{i}}$ and the Q_{scat} are plotted in Fig. 4 as a function of wavelength for a TiO_2 microspheres with d = 0.78 μm. The results show the internal energy is approximately 7.5 times higher than the energy at the focal volume of the illumination when the scattering is minimum at λ ~ 590 nm. This indicates that an induced excitation exists inside the sphere while very little radiation is scattered outside, which confirms the excitation of optical anapoles. The $\frac{W^{int}}{W^{i}}$ and the Q_{scat} of a TiO_2 microsphere with d = 0.88 μm is shown in Fig. S6 in the SI.

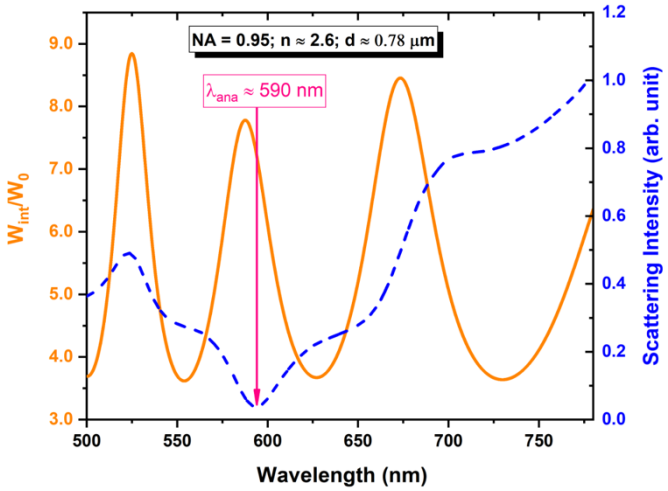

Figure 4: Calculated internal energy as a function of wavelength of a single TiO_2 microsphere with d ~ 0.78 μm under TFGB illumination with NA = 0.95. The internal energy of the particle is approximately 7.5 times higher than the energy of the illumination at the scattering minima at the anapole wavelength.

Note that unraveling dipolar regime, demonstration of close-to-zero back scattering, and excitation of nonradiating optical anapoles in mid-index mesoscale dielectric spheres do not appear simply because of scaling of dimension and refractive index as reducing refractive index would require larger sizes of the spheres to obtain similar results than high index nanoscale spheres. As discussed in section 2.1 and in Ref

[21], excitation of lossless dielectric spheres under PDF illumination leads to the emergence of pure electric (or magnetic) scattering regimes for $\sin\beta_1 = 0$ (or $\sin\alpha_1 = 0$), which give rise to $g = 0$, according to Eq. (2), for *y*-size parameter greater than 6. Hence, the results are relevant to only larger spheres/mesoscale regime at the optical frequencies. Therefore, these results imply that one can practically excite anapole states at any frequency in the optical regime, by changing the size parameter of the spheres within the "mesoscale regime" under dipolar excitation. For example, one should be able to observe nonradiating anapole state for a dielectric sphere with diameter, d = 0.78 mm, for (*i*) for n ~ 1.72 at ~ 547 nm (as shown in Fig S7 in the SI); (*ii*) for n ~ 2.04 at ~ 400 nm; (*iii*) for n ~ 2.43 at ~ 546 nm; (*iv*) for n ~ 3.13 at ~ 548 nm; and so on. For all these cases, the diameter of the sphere is exactly the same, that is, d = 0.78 μm (mesoscale regime); whereas the refractive index can vary from low- to mid- to high-index regime. Similarly, for example, for sphere with a specific refractive index, say, n ~ 2.43, one can excite anapole sates at any wavelength between 400 to 800 nm by varying the diameter from 0.5 to 1.2 μm.

3. Conclusion

In conclusion, we have unraveled dipolar regime, demonstrated close-to-zero backscattering, and excited non-radiating anapole states in mid-index titanium di-oxide (TiO_2, n ~ 2.6) dielectric spheres at the mesoscale regime under illumination with tightly focused Gaussian beams (TFGBs) for the first time. The ability to unravel dipolar regimes, and their associated effects in homogenous spheres in the mid-index regime at mesoscale would open up enormous possibilities in terms of availability of materials and their size parameters well beyond the current physical picture. Therefore, our result pushes the boundary of observation of nanophotonic phenomena to new regime with regards to type and size of the materials. This would lead to observation of interesting phenomena and applications, such as, electric and magnetic dipolar optical forces[70,71], radiation pressure[72], light transport phenomena[73], originally derived for small nanoparticles, can now be extended to mesoscale dielectric particles. Furthermore, the nonradiating properties of the anapole state as well as directional scattering in the form of maximum forward scattering by minimizing the backscattering can be potentially used to overcome the limitations of optical devices in terms of non-efficient coupling and directionality of light.

Acknowledgements

This material is based upon work supported in part by the National Science Foundation (NSF) under Grant No. DMR-2208240. The authors acknowledge usage of the FESEM facility in Material Research Laboratory (MRL) at University of Illinois Urbana Champaign. J.O.T. acknowledge support from Project No. PID2019-109905GA-C22 of the Spanish Ministerio de Ciencia, Innovación y Universidades (MICIU)

References

[1] L. Novotny, B. Hecht, Principles of Nano-Optics, Cambridge University Press, Cambridge, UK 2006, p. 3.

[2] A. B. Evlyukhin, S. M. Novikov, U. Zywietz, R. L. Eriksen, C. Reinhardt, S. I. Bozhevolnyi, B. N. Chichkov, *Nano Lett.* **2012**, *12*, 3749.

[3] A. I. Kuznetsov, A. E. Miroshnichenko, Y. H. Fu, J. Zhang, B. Luk'yanchuk, *Sci. Rep.* **2012**, *2*, 492.

[4] A. I. Kuznetsov, A. E. Miroshnichenko, M. L. Brongersma, Y. S. Kivshar, B. Luk'yanchuk, *Science* **2016,** *354*, aag2472.

[5] A. E. Miroshnichenko, A. B. Evlyukhin, Y. F. Yu, R. M. Bakker, A. Chipouline, A. I. Kuznetsov, B. Luk'yanchuk, B. N. Chichkov, Y. S. Kivshar, *Nat. Commun.* **2015**, *6*, 8069.

[6] V. A. Fedotov, A. V. Rogacheva, V. Savinov, D. P. Tsai, N. I. Zheludev, *Sci. Rep.* **2013**, *3*, 2967.

[7] S. Person, M. Jain, Z. Lapin, J. J. Saenz, G. Wicks, L. Novotny, *Nano Lett.* **2013**, *13*, 1806.

[8] Y. H. Fu, A. I. Kuznetsov, A. E. Miroshnichenko, Y. F. Yu, B. Luk'yanchuk, *Nat. Commun.* **2013**, *4*, 1527.

[9] P. Albella, M. A. Poyli, M. K. Schmidt, S. A. Maier, F. Moreno, J. J. Sáenz, J. Aizpurua, *J. Phys. Chem. C* **2013**, *117*, 13573.

[10] B. Rolly, B. Bebey, S. Bidault, B. Stout, N. Bonod, *Phys. Rev. B* **2012**, *85*, 245432.

[11] M. Caldarola, P. Albella, E. Cortés, M. Rahmani, T. Roschuk, G. Grinblat, R. F. Oulton, A. V. Bragas, S. A. Maier, *Nat. Commun.* **2015**, *6*, 7915.

[12] L. Zou, W. Withayachumnankul, C. M. Shah, A. Mitchell, M. Bhaskaran, S. Sriram, C. Fumeaux, *Opt. Express* **2013**, *21*, 1344.

[13] D. S. Filonov, A. E. Krasnok, A. P. Slobozhanyuk, P. V. Kapitanova, E. A. Nenasheva, Y. S. Kivshar, P. A. Belov, *Appl. Phys. Lett.* **2012**, *100*, 201113.

[14] a) O. V. Minin, I. V. Minin, *Photonics* **2021**, *8*, 591; b) I. V. Minin, O. V. Minin, *Photonics* **2022**, *9*, 762.

[15] A. B. Vasista, E. J. C. Dias, F. J. G. de Abajo, W. L. Barnes, *Nano Lett.* **2022**, *22*, 6737.

[16] L. Y. Yue, B. Yan, J. N. Monks, R. Dhama, C. L. Jiang, O. V. Minin, I. V. Minin, Z. B. Wang, *Sci. Rep.* **2019**, *9*, 20224.

[17] Z. B. Wang, B. Luk'yanchuk, L. Y. Yue, B. Yan, J. Monks, R. Dhama, O. V. Minin, I. V. Minin, S. M. Huang, A. A. Fedyanin, *Sci. Rep.* **2019**, *9*, 20293.

[18] N. I. Zheludev, G. H. Yuan, *Nat. Rev. Phys.* **2022**, *4*, 16.

[19] I. V. Minin, O. V. Minin, Y. Cao, B. Yan, Z. Wang, B. Luk'yanchuk, *Opto-Electron Sci* **2022**, *1*, 210008-1.

[20] L. Y. Yue, O. V. Minin, Z. B. Wang, J. N. Monks, A. S. Shalin, I. V. Minin, *Opt. Lett.* **2018**, *43*, 771.

[21] C. Sanz-Fernandez, M. Molezuelas-Ferreras, J. Lasa-Alonso, N. de Sousa, X. Zambrana-Puyalto, J. Olmos-Trigo, *Laser Photonics Rev.* **2021**, *15*, 2100035.

[22] J. Olmos-Trigo, D. R. Abujetas, C. Sanz-Fernandez, X. Zambrana-Puyalto, N. de Sousa, J. A. Sanchez-Gil, J. J. Saenz, *Phys. Rev. Res.* **2020**, *2*, 043021.

[23] M. Kerker, D.-S. Wang, C. L. Giles, *J. Opt. Soc. Am.* **1983**, *73*, 765.

[24] J. M. Geffrin, B. Garcia-Camara, R. Gomez-Medina, P. Albella, L. S. Froufe-Perez, C. Eyraud, A. Litman, R. Vaillon, F. Gonzalez, M. Nieto-Vesperinas, J. J. Saenz, F. Moreno, *Nat. Commun.* **2012**, *3*, 1171.

[25] K. Kim, E. Wolf, *Opt. Commun.* **1986**, *59*, 1.

[26] A. J. Devaney, E. Wolf, *Phys. Rev. D* **1973**, *8*, 1044.

[27] D. Bohm, M. Weinstein, *Phys. Rev.* **1948**, *74*, 1789.

[28] P. Pearle, *Foundations of Physics* **1978**, *8*, 879.

[29] N. A. Nemkov, A. A. Basharin, V. A. Fedotov, *Phys. Rev. B* **2017**, *95*, 165134.
[30] C. W. Hsu; B. Zhen; A. D. Stone; J. D. Joannopoulos; M. Soljacic, *Nat. Rev. Mater.* **2016**, *1*, 16048.
[31] F. Monticone, A. Alu, *Phys. Rev. Lett.* **2014**, *112*, 213903.
[32] K. V. Baryshnikova, D. A. Smirnova, B. S. Luk'yanchuk, Y. S. Kivshar, *Adv. Opt. Mater.* **2019**, *7*, 1801350.
[33] K. Koshelev, G. Favraud, A. Bogdanov, Y. Kivshar, A. Fratalocchi, *Nanophotonics* **2019**, *8*, 725.
[34] F. Monticone, D. Sounas, A. Krasnok, A. Alu, *ACS Photonics* **2019**, *6*, 3108.
[35] W.-C. Zhai, T.-Z. Qiao, D.-J. Cai, W.-J. Wang, J.-D. Chen, Z.-H. Chen, S.-D. Liu, *Opt. Express* **2016**, *24*, 27858.
[36] G. Grinblat, Y. Li, M. P. Nielsen, R. F. Oulton, S. A. Maier, *ACS Nano* **2017**, *11*, 953
[37] L. Xu, M. Rahmani, K. Z. Kamali, A. Lamprianidis, L. Ghirardini, J. Sautter, R. Camacho-Morales, H. T. Chen, M. Parry, I. Staude, G. Q. Zhang, D. Neshev, A. E. Miroshnichenko, *Light: Sci. Appl.* **2018**, *7*, 44.
[38] J. S. T. Gongora, A. E. Miroshnichenko, Y. S. Kivshar, A. Fratalocchi, *Nat. Commun.* **2017**, *8*, 15535.
[39] T. H. Feng, Y. Xu, W. Zhang, A. E. Miroshnichenko, *Phys. Rev. Lett.* **2017**, *118*, 173901.
[40] R. Wang, L. Dal Negro, *Opt. Express* **2016**, *24*, 19048.
[41] M. Gupta, Y. K. Srivastava, M. Manjappa, R. Singh, *Appl. Phys. Lett.* **2017**, *110*, 121108.
[42] A. K. Ospanova, I. V. Stenishchev, A. A. Basharin, *Laser Photonics Rev.* **2018**, *12*, 1800005.
[43] S. D. Liu, Z. X. Wang, W. J. Wang, J. D. Chen, Z. H. Chen, *Opt. Express* **2017**, *25*, 22375.
[44] A. A. Basharin, V. Chuguevsky, N. Volsky, M. Kafesaki, E. N. Economou, *Phys. Rev. B* **2017**, *95*, 035104.
[45] Y. Q. Yang, V. A. Zenin, S. I. Bozhevolnyi, *ACS Photonics* **2018**, *5*, 1960.
[46] Y. B. Zhang, W. W. Liu, Z. C. Li, Z. Li, H. Cheng, S. Q. Chen, J. G. Tian, *Opt. Lett.* **2018**, *43*, 1842.
[47] J. H. Yan, X. Y. Liu, C. R. Ma, Y. C. Huang, G. W. Yang, *Mater. Sci. Eng., R* **2020**, *141*, 100563.
[48] J. Olmos-Trigo, M. Melendez, R. Delgado-buscalioni, J. J. Saenz, *Opt. Express* **2019**, *27*, 16384.
[49] J. Olmos-Trigo, C. Sanz-Fernandez, A. Garcia-Etxarri, G. Molina-Terriza, F. S. Bergeret, J. J. Saenz, *Phys. Rev. A* **2019**, *99*, 013852.
[50] I. Fernandez-Corbaton, X. Zambrana-Puyalto, N. Tischler, X. Vidal, M. L. Juan, G. Molina-Terriza, *Phys. Rev. Lett.* **2013**, *111*, 060401.
[51] P. Wozniak, P. Banzer, G. Leuchs, *Laser Photonics Rev.* **2015**, *9*, 231.
[52] J. A. Parker, H. Sugimoto, B. Coe, D. Eggena, M. Fujii, N. F. Scherer, S. K. Gray, U. Manna, *Phys. Rev. Lett.* **2020**, *124*, 097402.
[53] X. Zambrana-Puyalto, X. Vidal, P. Wozniak, P. Banzer, G. Molina-Terriza, *ACS Photonics* **2018,** *5*, 2936.
[54] H. C. Hulst, H. C. van de Hulst, Light Scattering by Small Particles, Courier Corporation, North Chelmsford, MA, USA 1957.
[55] J. Olmos-Trigo, C. Sanz-Fernandez, F. S. Bergeretm J. J. Saenz, *Opt. Lett.* **2019**, *44*, 1762.
[56] X. Zambrana-Puyalto, X. Vidal, G. Molina-Terriza, *Opt. Express* **2012**, *20*, 24536.
[57] C. Bohren, D. Huffmann, Absorption and Scattering of Light by Small Particles, John-Wiley, New York, USA 1983.
[58] C. Zaza, I. L. Violi, J. Gargiulo, G. Chiarelli, L. Schumacher, J. Jakobi, J. Olmos-Trigo, E. Cortes, M. Konig, S. Barcikowski, S. Schlucker, J. J. Saenz, S. A. Maier, F. D. Stefani, *ACS Photonics* **2019**, *6*, 815.
[59] C. H. Huang, T. Kudo, R. Bresoli-Obach, J. Hofkens, T. Sugiyama, H. Masuhara, *Opt. Express* **2020**, *28*, 27727.

[60] I. Aibara, C. H. Huang, T. Kudo, R. Bresoli-Obach, J. Hofkens, A. Furube, H. Masuhara, *J. Phys. Chem. C* **2020**, *124*, 16604.
[61] L. Allen, M. W. Beijersbergen, R. J. C. Spreeuw, J. P. Woerdman, *Phys. Rev. A* **1992**, *45*, 8185.
[62] N. M. Mojarad, V. Sandoghdar, M. Agio, *J. Opt. Soc. Am. B* **2008**, *25*, 651.
[63] S. Orlov, U. Peschel, T. Bauer, P. Banzer, *Phys. Rev. A* **2012**, *85*, 063825.
[64] X. Zambrana-Puyalto, *arXiv:1502.01648* **2016**.
[65] https://www.epruibiotech.com/product/tio2-microspheres/
[66] A. Bendavid, P. J. Martin, *J. Aust. Ceram. Soc.* **2014**, *50*, 86.
[67] U. Manna, J. H. Lee, T. S. Deng, J. Parker, N. Shepherd, Y. Weizmann, N. F. Scherer, *Nano Lett.* **2017**, *17*, 7196.
[68] U. Manna, H. Sugimoto, D. Eggena, B. Coe, R. Wang, M. Biswas, M. Fujii, *J. Appl. Phys.* **2020**, *127*, 033101.
[69] V. Savinov, N. Papasimakis, D. P. Tsai, N. I. Zheludev, *Commun. Phys.* **2019**, *2*, 69.
[70] S. Albaladejo, M. I. Marques, M. Laroche, J. J. Saenz, *Phys. Rev. Lett.* **2009**, *102*, 113602.
[71] O. M. Marago, P. H. Jones, P. G. Gucciardi, G. Volpe, A. C. Ferrari, *Nat. Nanotechnol.* **2013**, *8*, 807.
[72] A. Y. Bekshaev, K. Y. Bliokh, F. Nori, *Phys. Rev. X* **2015**, *5*, 011039.
[73] R. Gomez-Medina, L. S. Froufe-Perez, M. Yepez, F. Scheffold, M. Nieto-Vesperinas, J. J. Saenz, *Phys. Rev. A* **2012**, *85*, 035802.

Conflict of Interest

The authors declare no conflict of interest.

TABLE OF CONTENTS

ToC text: In this manuscript, we study light-matter interactions of relatively low-index wavelength-scaled dielectric particles. More specifically, we unravel dipolar regime, demonstrate close-to-zero backscattering, and excite non-radiating anapole states in mid-index dielectric spheres at the mesoscale regime. Our results would open up enormous possibilities in terms of availability of materials and their size parameters well beyond the current physical picture.

ToC Figure: